Normal-State Properties of Uniaxially Pressed $Bi_{1.65}Pb_{0.35}Sr_2Ca_2Cu_3O_{10+\delta}$ Ceramics

E. Govea-Alcaide,

Instituto de Física, Universidade de São Paulo, CP 66318, 05315-970, São Paulo, SP, Brazil and
Departamento de Física, Universidad de Oriente, Patricio Lummumba s/n, P. O. Box 90500, Santiago de Cuba, Cuba

P. Muné,

Departamento de Física, Universidad de Oriente, Patricio Lummumba s/n, P. O. Box. 90500, Santiago de Cuba, Cuba

and R. F. Jardim

Instituto de Física, Universidade de São Paulo, CP 66318, 05315-970, São Paulo, SP, Brazil

We have studied the effects of the uniaxial compacting pressure on the physical properties of polycrystalline $Bi_{1.65}Pb_{0.35}Sr_2Ca_2Cu_3O_{10+\delta}$ (Bi-2223) superconductors. Powders of this material were pressed at different uniaxial compacting pressures ranging from ~ 90 to ~ 600 MPa and heat-treated at the same temperature. A characterization of samples by using Scanning Electron Microscopy and X-ray diffractometry indicated an appreciable improvement of the degree of texture with increasing pressure. The temperature dependence of the electrical resistivity $\rho(T)$ exhibits a T-linear behavior at temperatures higher than $T^* \sim 235$ K. The deviation of $\rho(T)$ from the linear behavior below T^* indicates the opening of the pseudogap, a feature confirmed by magnetic susceptibility measurements performed in powder samples. From linear fittings of the normal-state electrical resistivity we were able to separate contributions to $\rho(T)$ arising from both the grain misalignment and microstructural defects. The results suggest that the grain orientation and the connectivity between them are improved with increasing compacting pressure. Also, based on the linearity of the electrical resistivity data both the transport electron-phonon coupling constant, λ_{tr}, and the mean free path, l, were estimated. We have found that in the sample with the highest degree of texture $\lambda_{tr} \sim 0.53$, a value comparable with the one obtained in Bi-2223 single crystals. However, the result for $l \sim 12.7$ Å at 300 K, in the same ceramic sample, is close to 3 times lower than the single crystal value. The influence of the intergranular electrical resistivity in determining band-theory parameters was analyzed within the framework of a current conduction model for granular superconducting materials.

I. INTRODUCTION

The presence of grain boundaries in various forms of polycrystalline superconducting samples (bulk sintered material, thick films, tapes, and wires) is a natural consequence of the preparation conditions from powdered precursors. Grain boundaries play an important role in limiting the general transport properties of polycrystalline superconductors. Moreover, it is well established that the properties of grain boundaries mainly control the macroscopic properties of all high-T_c materials.[1] This phenomenon is mainly attributed to the misorientation between the grains usually referred to as the *mesotexture*.[2] High angle grain boundaries can act as Josephson coupled weak links, leading to a significant field-dependent suppression of the supercurrent across the grain boundary.[1] In order to improve the transport properties of these materials they are subjected to large mechanical deformations. These techniques have proven to be effective in raising the superconducting critical current J_c of the superconducting tapes,[3–5] mainly due to a marked increase in both the *meso-texture* and the *micro-texture*, where the latter is related to the orientation of the individual grains regarding the direction in along the mechanical deformation is applied. The combination of the above types of texture gives the *macro-texture* of the material.[2]

In a previous work, we have described a systematic study concerning the influence of uniaxial compacting pressure on the general superconducting properties of polycrystalline (Bi-Pb)$_2$Sr$_2$Ca$_2$Cu$_3$O$_{10+\delta}$ (Bi-2223) samples.[6] By performing measurements of critical current density as a function of applied magnetic field, $J_c(B_a)$, we have observed three different superconducting levels: the superconducting grains, the superconducting clusters, and the weak links. It was found that properties of the last two levels are very sensitive to the compacting pressure, mostly due to changes in the grain boundary properties. However, a similar systematic study regarding effects of the uniaxial compacting pressure on the normal-state transport properties of the above ceramic material is lacking.

The normal state properties of high-T_c superconductors, such as the temperature dependence of the electrical resistivity, $\rho(T)$, have been an attractive topic for investigations in the last years. This occurs because it is possible to obtain some important parameters such as the electron-phonon coupling constant, λ_{tr}, and the mean free path, l, by correlating transport measurements with band-theory arguments.[7] In granular superconducting materials, studies involving the behavior of $\rho(T)$ present an additional inconvenient due to the complexity of their microstructure in which both intragranular and intergranular contributions as well as the degree of texture and structural defects must be considered.[13] Consequently, estimates of band-theory parameters such as λ_{tr} and l from $\rho(T)$ data of ceramic samples require corrections in order to separate the influence of microstructural contributions on the intrinsic electrical resistivity of the Cu-O planes, also referred

TABLE I: Few parameters of the uniaxially compacting pressed samples studied in this work: the compacting pressure, **P**, the offset superconducting critical temperature, T_{off}, the electrical resistivity at 300 K, $\rho(300\ K)$, and the paracoherent electrical resistivity, ρ_p.

Sample	P(MPa)	T_{off}(K)	$\rho(300K)$(mΩ cm)	ρ_p(mΩ cm)
P1	98	99.8	2.88	0.69
P2	196	101.5	2.19	0.54
P3	294	102.5	1.81	0.42
P4	490	102.8	1.63	0.36
P5	588	103.0	1.24	0.28

to as in-plane electrical resistivity ρ_{ab}. Within this context, Gurvitch *et al.*[7] have corrected the electrical resistivity data of both La$_{2-x}$Sr$_x$CuO$_4$ and YBa$_2$Cu$_3$O$_{7-\delta}$ ceramic samples by using a constant factor of ~ 2 and comparing the results with data obtained in high-quality ceramics and epitaxial thin films.

In addition, electrical resistivity measurements in the normal-state of cuprates have revealed the presence of electronic correlations at high temperatures, referred to as the pseudogap. Such a pseudogap, which manifests itself as a depletion of the quasiparticle density of states (DOS) below a characteristic temperature T^*,[8] would reflect the creation of a precursor state of the Cooper pairing [9] that acquires long-range coherence order below the superconducting critical temperature, T_c. The pseudogap temperature, T^*, can be estimated by using different techniques such as the temperature dependence of the electrical resistivity, $\rho(T)$, and magnetic susceptibility, $\chi(T)$.[8, 10] In fact, T^* can be inferred from deviations in both $\rho(T)$ and $\chi(T)$ data from the expected behavior at temperatures well above T$_c$.[8] In addition, it is well known that the magnetic susceptibility behavior is related to the Pauli paramagnetic susceptibility of the Cu^{2+} spins, which in turn is related to the density of state at the Fermi level.[11, 12]

In this work we focus on the $\rho(T)$ measurements of polycrystalline Bi$_{1.65}$Pb$_{0.35}$Sr$_2$Ca$_2$Cu$_3$O$_{10+\delta}$ samples subjected to different uniaxial compacting pressures before the last heat treatment. X-ray diffraction patterns, XRD, taken on powder and bulk samples, micrographies by Scanning Electron Microscope, SEM, taken on free surface and fracture, and measurements of magnetization versus temperature, $M(T)$, have been performed as complementary characterizations. The main contribution of this paper is to quantify the effects of uniaxial compacting pressure on the $\rho(T)$ dependence mainly in the normal-state region. By using the model proposed by Gurvitch *et al.*[7] some relevant parameters were extracted such as the electron-phonon coupling constant and the mean free path. The resulting values have been also analyzed within the framework of the current conduction model proposed by Díaz *et al.*.[13]

II. EXPERIMENTAL PROCEDURE

Polycrystalline samples of the superconductor Bi$_{1.65}$Pb$_{0.35}$Sr$_2$Ca$_2$Cu$_3$O$_{10+\delta}$ (Bi-2223) were prepared from powders of Bi$_2$O$_3$, PbO, SrCO$_3$, CaCO$_3$, and CuO, which were mixed in an atomic ratio of Pb:Bi:Sr:Ca:Cu (0.35:1.65:2:2:3). Details of the sample preparation process are described elsewhere.[6] Here, before the last heat treatment, the powders were uniaxially pressed at different compacting pressures ranging from ~ 90 to ~ 600 MPa (see Table I), and the typical dimensions of the pellets were $d = 10$ mm in diameter and $h = 1$ mm in height. The last heat treatment of the pellets was performed in air at 845 °C for 40 h followed by slow cooling.

We have evaluated the phase identification in both powder and bulk samples by means of X-ray diffraction patterns obtained in a Bruker-AXS D8 Advance diffractometer. Also, a qualitative evaluation of the degree of texture in pellet samples was made by using the same technique. These measurements were performed at room temperature using Cu Kα radiation in the $3° \leq 2\theta \leq 80°$ range with a 0.02° (2θ) step size and 5 s counting time.

The microstructure of fractured and free surfaces of samples was observed by using a JEOL JSM-5800 Scanning Electron Microscope operating at 25 kV. In the first type of measurement we have observed the shape of the grains, their degree of orientation, and estimated the their mean size. From the second one, we qualitatively evaluated the porosity of samples subjected to different compacting pressures.

We have performed dc magnetization measurements $M(T)$ in powders extracted from each pellet and with identical mass, by using a commercial Quantum Design SQUID magnetometer. The powders were cooled in zero applied magnetic field from room temperature down to 10 K. After this step, zero-field cooled (ZFC) and field-cooled (FC) measurements were performed under applied magnetic fields and up to 300 K.

The temperature dependence of the electrical resistivity, $\rho(T)$, was measured by using the standard dc four-probe technique in slabs with typical dimensions of $t = 0.5$ mm (thickness), $w = 2$ mm (width), and $l = 10$ mm (length). These measurements were performed by applying the excitation current along the plane of the sample perpendicular to the direction in which the uniaxial compacting pressure has been applied. After cooling the sample in zero applied magnetic field down to 77 K, an excitation current of 1 mA was applied. The specimen was then warmed slowly from 77 K to room temperature and both the voltage across the sample and the temperature were collected.

Current-voltage (*I-V*) measurements were performed to determine the paracoherent electrical resistivity, ρ_p, of the samples.[13] We have used the so-called quasi-dc four-probe technique in these experiments, as described in Ref. 14. Once the sample was cooled down and fixed at a given temperature close to 103 K, an excitation current, I_{ex}, was applied during 1 sec and the voltage across the sample, V, was measured. After this step, I_{ex} was turned off during ~ 10 sec, avoiding possible Joule self-heating effects, and the voltage was measured again for a new value of I_{ex}. Repetitions of the above steps accom-
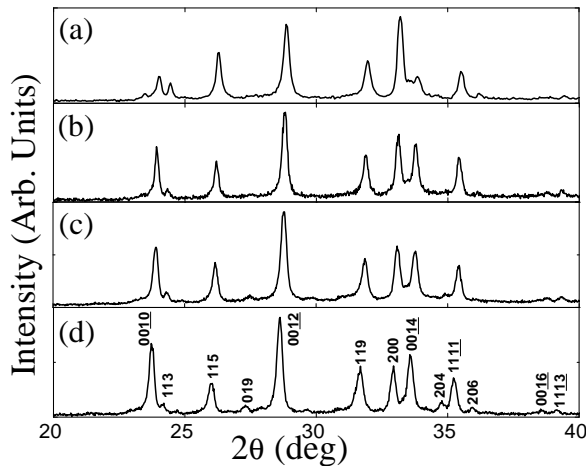
FIG. 1: X-ray diffraction patterns of a powder sample (a), and bulk samples subjected to different compacting pressures: **P2**(b), **P3**(c), and **P5**(d). The reflections belonging to the Bi-2223 phase are marked by Miller indexes in (d).
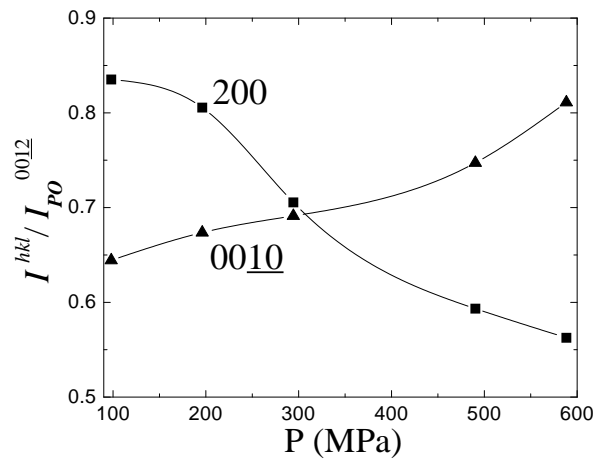

FIG. 2: Relative intensity dependence of the Bragg reflections (0010) and (200) with increasing compacting pressure. Lines between points are guides for eyes.

panied by a continuous increase of the excitation current resulted in several $I-V$ curves at different temperatures. From the results, ρ vs. J curves are built and ρ_p is extracted from the apparent observed plateau in the ρ vs. J dependence.[13] By using this procedure, the electrical resistivity of the sample ρ and the transport current density flowing through the material $J = I_{ex}/(wt)$ are determined.

III. EXPERIMENTAL RESULTS

Figure 1 displays the X-ray diffraction patterns taken on bulk samples **P2**, **P3**, and **P5**, and in a powder sample **PO**. This powder was prepared from the sample **P2**, that was reground after the last heat treatment. A comparative analysis of these patterns reveals that all samples have similar chemical composition and that all the indexed reflections are related to the high-T_c Bi-2223 phase. The unit-cell parameters were calculated regarding an orthorhombic unit cell and the obtained values $a = 5.410$ Å, $b = 5.413$ Å, and $c = 37.152$ Å are in excellent agreement with those reported for the same compound elsewhere.[15] The values of a, b, and c were found to be essentially the same for the samples subjected to different compacting pressures. A careful inspection of these X-ray diagrams also reveal clear effects related to the increase of the compacting pressure. A typical example is associated with changes observed, for instance, in the evolution of the (200) and (0014) peaks. The data indicate a monotonic increase of the relative intensity of the (0014) peak with increasing compacting pressure. This strong suggest that the grains belonging to samples subjected to higher compacting pressures are more aligned along the c-axis, a feature that is corroborated by the continuous decrease of the relative intensity related to the reflection (200).

In order to quantify these features, we have also computed the relative intensity of both (0010) and (200) Bragg peaks re-

garding the intensity of the reflection (0012) belonging to the powder sample **PO**. The compacting pressure dependence of both reflections are displayed in Fig. 2. The data indicate that the relative height of the peak (0010) increases monotonically with increasing compacting pressure suggesting that higher compacting pressures improved the degree of texture and results in a better alignment of the grains. In addition, it seems that grains are aligned with their c-axis preferentially parallel to the compacting direction. Indeed, such a feature is consistent with the progressive decrease of the relative intensity related to the peak (200), as inferred from the data shown in Fig. 2.

The effect of the compacting pressure has its counterpart in the microstructure of these samples. This can be inferred from the free surface and the fracture micrographs of samples **P1** and **P5** which are shown in Fig.3. In both types of micrographs it is possible to observed that the granular morphology of both samples is similar, exhibiting the occurrence of grains with nearly platelet-like shape. Also, a careful inspection of the free surface micrographies of samples **P1** and **P5** (see Figs. III) and III) reveals that the later is more homogeneous, mostly due to a marked reduction in the porosity level with increasing compacting pressure.

The analysis of fracture micrographies in these samples also indicates changes in both the grain size and the grain orientation. The average grain size in the sample **P1** was found to be $L_a = 6$ μm long and as thick as $L_c = 0.3$ μm. For the sample **P5**, the grains were found to have dimensions of $L_a = 4$ μm long and $L_c = 0.1$ μm thick. The ratio L_a/L_c, which is referred to as the mean aspect ratio of the grains,[13] has been found to be very sensitive to the applied pressure and were $\sim$ 20 and $\sim$ 40 for the samples **P1** and **P5**, respectively. These values are higher than those of 2.5 and 4.5 in ceramic samples of $YBa_2Cu_3O_{7-\delta}$,[13] but similar to the one of $\sim$ 50 estimated in (Bi,Pb)-2223 superconducting tapes.[2]

On the other hand, the micrograph belonging to the sample **P1** (Fig.III) reveals that the grains are random oriented and
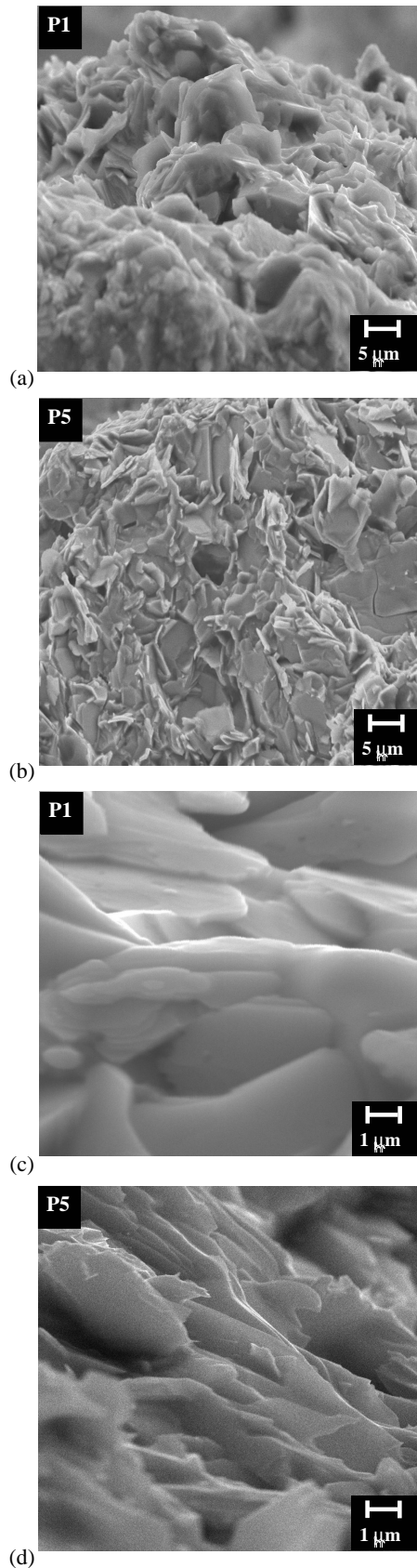
(a)

(b)

(c)

(d)

FIG. 3: Micrographs of the free surfaces (III and III), and fractured samples (III and III) **P1** and **P5**, respectively, which were subjected to different uniaxial compacting pressures, as displayed in Table I.

thicker than those, for instance, of the sample **P5**, which are thinner and aligned parallel to each other. The above results are in excellent agreement with the XRD analysis discussed above, which indicated a continuous increase of the degree of texture with increasing compacting pressure.
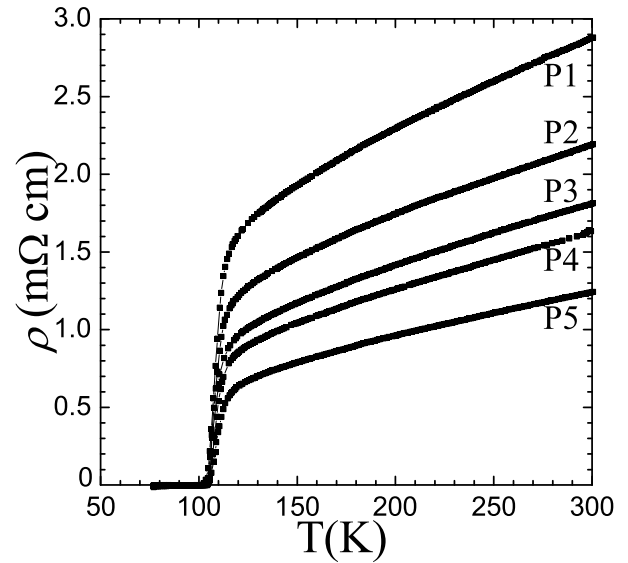

FIG. 4: Temperature dependence of the electrical resistivity of the samples **P1**, **P2**, **P3**, **P4**, and **P5**. The results show a progressive decrease of $\rho(T)$ with increasing compacting pressure. Some physical parameters of the samples extracted from these $\rho(T)$ curves are displayed in Table I and discussed in the text.

It is reasonable to point out that the morphological alterations provoked by increasing the compacting pressure must be reflected in some macroscopic properties of these ceramic samples as the temperature dependence of the electrical resistivity. Following this statement, the temperature dependence of the electrical resistivity $\rho(T)$ of samples **P1**, **P2**, **P3**, **P4**, and **P5** are displayed in Fig. 3. All curves exhibit a transition to the superconducting state bellow the onset superconducting critical temperature $T_{on} \sim 110$ K. Such a critical temperature is identified as the transition of isolated grains to the superconducting state in granular superconductors. The observation of an almost constant value of $T_{on} \sim 110$ K in all samples suggests that the superconducting grains seem to be insensitive to the increasing of the compacting pressure, at least in the pressure range used in these experiments. In addition, a nearly constant value of $T_{on} \sim 110$ K, combined with the XRD results which exhibited absence of Bragg peaks belonging to extra phases, indicates that the grains of all samples have essentially the same stoichiometry.

We have also found that the temperature in which the zero resistance state is attained, T_{off}, slightly increases with increasing compacting pressure (see Table I). Since T_{off} is close related to the intergranular component of these ceramic samples, the $\rho(T)$ data indicate that increasing compacting pressure results in a better connectivity between grains, besides the higher alignment along the *ab*-plane, as inferred from the data shown above. On the other hand, the $\rho(T)$ curves

exhibit a clear metallic-like behavior in the normal-state region. Such a result, along with the progressive decrease of the magnitude of $\rho(T)$ at 300 K (see Table I), suggests that the electrical current flows preferentially along the *ab*-plane of the partially oriented grains in these samples.

The $\rho(T)$ data were found to obey a linear trend in a well defined temperature range. Thus, a relevant question concerns the procedure to determine the temperature in which $\rho(T)$ curves start to deviate from linearity. Usually, this temperature is determined by visual localization. However, such a procedure is too subjective to be quantitative, as discussed by Tallon *et al.*.[8] In order to evaluate the deviation from linearity of our $\rho(T)$ data, we have computed several slopes $\Delta\rho(T)/\Delta T$ following the relation

$$m(T) = \frac{\rho(300K) - \rho(T)}{300K - T}, \qquad (1)$$

where $\rho(300 \text{ K})$ is the electrical resistivity at 300 K (see Table I). The temperature T was increased from 160 K to 260 K, in step sizes of ~ 5 K. A linear dependence of $\rho(T)$ data implies, according to Eq. (1), a temperature-independent behavior of the $m(T)$ dependence.
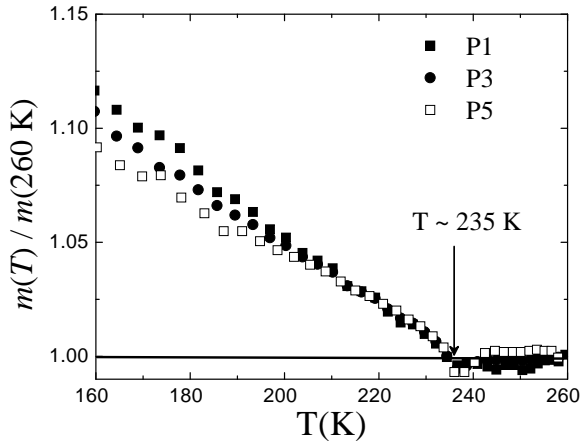

FIG. 5: Normalized values of $m(T)$, calculated by using the Eq. 1 from 160 to 260 K, as a function of temperature. A constant value of of $m(T)$ is observed for temperatures higher than 235 K, as discussed in the text.

The temperature dependence of the normalized $m(T)$ curves of the samples **P1**, **P3**, and **P5** are displayed in Figure 5. The $m(T)$ curves exhibit a temperature independent behavior from room temperature down to $T_\rho^* \approx 235$ K. Below T_ρ^*, the $m(T)$ curves of samples **P1**, **P3**, and **P5** display a similar behavior and start to deviate each other at a lower temperature $T \approx 210$ K. Thus, a temperature-independent behavior in the $m(T)$ dependence indicates that all $\rho(T)$ curves have a T-linear behavior in a narrow temperature range, or more appropriately, from $T_\rho^* \approx 235$ K to 300 K. The data shown in Fig. 4 also indicate that T_ρ^* seems to be insensitive to changes in the compacting pressure.

As already mentioned, it is well accepted that such a T-linear deviation in $\rho(T)$ curves at higher temperatures consti-
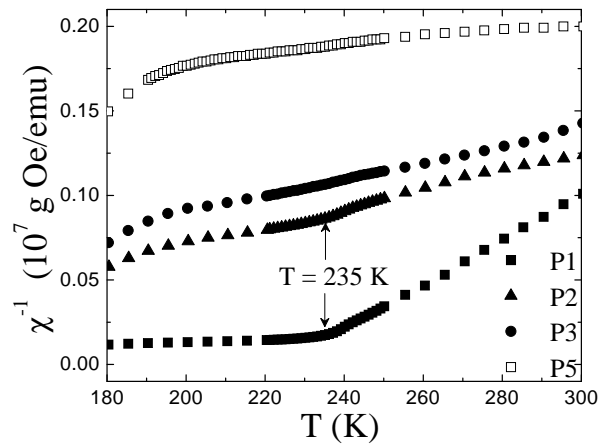

FIG. 6: Temperature dependence of the inverse magnetic susceptibility $\chi^{-1}(T)$ measured in samples **P1**, **P2**, **P3**, and **P5**.

tutes an evidence of the pseudogap opening. Also, it has been pointed out that this deviation may be reflected in the density of the states at the Fermi surface due to the Cooper pair formation without long-range phase coherence.[9] In order to verify the above statement, magnetic susceptibility measurements were performed in powder samples. Figure 6 displays the temperature dependence of the inverse magnetic susceptibility, $\chi^{-1}(T)$, of samples **P1**, **P2**, **P3**, and **P5**. The curves show a clear deviation from linearity of the Curie-type magnetic susceptibility behavior at $T_\chi^* \approx 235$ K, a feature which is much more pronounced in samples subjected to low compacting pressures as **P1** and **P2**.

With the aim to discuss the differences between the $\chi^{-1}(T)$ curves of our batch of samples, simple and qualitative arguments can be used. A continuous decrease in temperature would result in two opposite effects on the magnetic susceptibility of the paramagnetic state: (1) a better alignment of the magnetic dipoles along the direction of the applied magnetic field due to the decrease of the thermal energy (Curie law), and (2) a decrease in the number of magnetic dipoles at temperatures below T^* because part of them participate in the creation of Cooper pairs, which have dipole momentum equal to zero. Within this scenario, the creation of Cooper pairs results in a decrease of the density of states and, consequently, a decrease in the Pauli paramagnetic susceptibility term. On the other hand, the intensity with both effects are reflected in $\chi^{-1}(T)$ curves depends on the demagnetizing factors of the grains in the powder samples. As shown in figures III and III, the granular morphology of these samples has been altered with increasing compacting pressure: it evolves from grains with nearly ellipsoidal shape (see sample **P1**) to grains with a platelet-like shape (see sample **P5**). In fact, the average value of the grain thickness, L_c, for the sample **P1** is close to three times larger than the one observed in the sample **P5**. The other dimensions of the grains were found to be similar in both samples. Therefore, increasing compacting pressure provokes a decrease in the average value of the demagnetizing factor of the grains and, as consequence, a decrease in the

measured values of the magnetic susceptibility. Thus, the deviation from the Curie law below $T_\chi^* \approx 235$ K is expected to be much less pronounced in samples subjected to higher compacting pressures, as observed in our experiments. Our value of $T_\chi^* \approx 235$ K agrees well with the pseudogap temperature reported by both Fujii *et al.* [10] and Yamada *et al.* [16] in $Bi_2Sr_2Ca_2Cu_3O_{10+\delta}$ single crystals, as well as by Ekino *et al.* [17] in $(Bi\text{-}Pb)_2Sr_2Ca_2Cu_3O_{10+\delta}$ ceramic samples. Thus, our combined results of transport and magnetic measurements suggest that changes in $T = T_\rho^* \approx T_\chi^* \approx 235$ K are related to the opening of the pseudogap at this temperature.
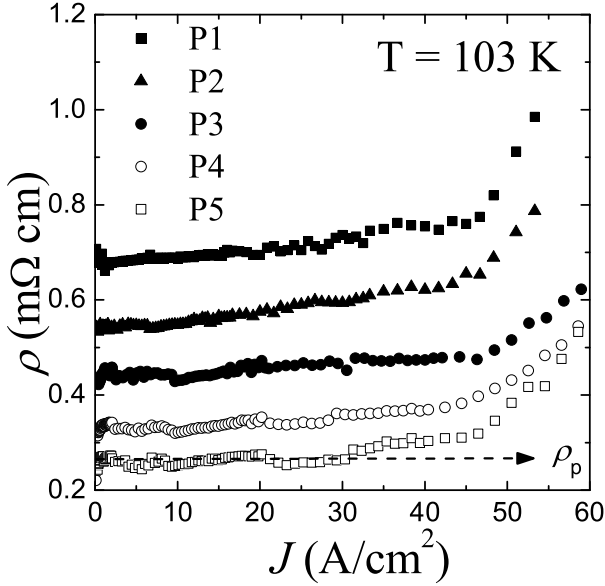

FIG. 7: ρ vs. J curves for all samples studied in this work. The paracoherent electrical resistivity ρ_p has been determined from the apparent linear plateau of the $\rho(J)$ curves, as indicated by the dashed line of the curve belonging to the sample **P5**.

Another important information regarding the effects of compacting pressure on the intergranular features of samples can be extracted from the paracoherent electrical resistivity, ρ_p. As reported by Díaz *et al.*,[13] effects arising from the misalignment of grains in transport data can be disregarded in the paracoherent state because the grains are in the superconducting state while the intergranular junctions remain in the normal state. In order to determine the paracoherent electrical resistivity of our samples, ρ vs. J curves were measured and the results are shown in Figure 7. Values of ρ_p were extracted by extrapolating the apparent observed plateau in the ρ vs. J behavior[13] and are shown in Table I. Even when the values of ρ were very scattered we were able to verify the existence of an almost constant value of ρ for $J \leq 45$ A/cm^2. In addition, the data indicate a progressive decrease in ρ_p with increasing compacting pressure, as confirmed by the estimated values of $\rho_{p1} = 0.69$ mΩ cm and $\rho_{p5} = 0.28$ mΩ cm in samples **P1** and **P5**, respectively. These results indicate that increasing compacting pressure improves the intergranular components of these uniaxially pressed Bi-2223 samples.

The ρ vs. J curves also displays a departure from the

plateau observed close to $J \approx 45$ A/cm^2 in all samples. As discussed in Ref. 13, such a value would be related to the superconducting critical current density of the grains, J_{cg}. However, such a value seems to be very low as compared with those of $J_{cg} \approx 10^3$-10^4 A/cm^2 obtained by magnetic measurements in similar temperatures.[18, 19] Such a discrepancy is related to the anisotropic factor J_{cg}^{ab}/J_{cg}^c, where J_{cg}^{ab} and J_{cg}^c are the in-plane and out-of-plane superconducting critical current densities of grains, respectively. In Bi-2223 compounds $J_{cg}^{ab}/J_{cg}^c \sim 50$, as reported elsewhere.[20] Within this context, one would expect that the first change in the plateau of $\rho(J)$ curves reflects the dissipation in grains mainly oriented along the *c*-axis parallel to the applied current density, i.e., this value corresponds to J_{cg}^c. By assuming that the values of the critical current density reported by magnetic measurements [18, 19] mainly reflect the J_{cg}^{ab} component, then our results for the out-of-plane J_c seem to be reasonable.

IV. DISCUSSION

The influence of the uniaxial compacting pressure on the normal-state transport properties has been clearly demonstrated in XRD, SEM, and $\rho(T)$ measurements (see Figs. 2-4). The combined results indicate an increase of both the degree of texture (grain alignment) and the grain connectivity of the samples. Thus, a comprehensive analysis of these effects on the transport properties must be considered.

As far as this point is concerned, Díaz *et al.* [13] have proposed a model in which the $\rho(T)$ data of polycrystalline samples of high temperature superconductors are believed to be strongly influenced by two different contributions: one associated with the misalignment of the grains (texture degree) and the other one related to microstructural defects such as voids and microcracks. Within the context of the model, the $\rho(T)$ dependence can be written as[13]

$$\rho(T) = \frac{1}{\alpha_n}(\rho_{ab} + \rho_{wl}), \quad (2)$$

where

$$\alpha_n = f\alpha_{str} \quad (3)$$

is a factor that enhances the electrical resistivity due to both the misalignment of the grains f; $0 < f \leq 1$; and microstructural defects α_{str}; $0 < \alpha_{str} \leq 1$.

In such a model, the grains are believed to behave as a single crystal. Then, the first term in the Eq. (2) is related to the average electrical resistivity of the *ab*-plane, ρ_{ab}. The second one, ρ_{wl}, is the actual average of the intergranular component, which is assumed to be temperature-independent. In our analysis, the term ρ_{ab} has been assumed to be linearly temperature-dependent and zero-residual temperature intercept. In fact, Fujii *et al.* [10] have reported measurements of both the in-plane $\rho_{ab}(T)$ and the out-of-plane $\rho_c(T)$ electrical resistivity as a function of temperature in $Bi_2Sr_2Ca_2Cu_3O_{10+\delta}$

TABLE II: Parameters obtained by the linear fitting of the $\rho(T)$ curves: A is the slope of the electrical resistivity data in the T-linear region and $\rho(0)$ the residual electrical resistivity. We have also included the parameters obtained by using the model proposed in Ref. 13. Here ρ_{wl} is the average intergranular electrical resistivity and α_n a factor that enhances the electrical resistivity due to the grain misalignment, f, and microstructural defects, α_{str}.

Sample	$A(\mu\Omega\text{cm/K})$	$\rho(0)(\text{m}\Omega\text{cm})$	$\rho_{wl}(\text{m}\Omega\text{cm})$	α_n	f	α_{str}
P1	5.62	1.19	0.39	0.33	0.58	0.57
P2	4.32	0.89	0.38	0.43	0.61	0.70
P3	3.82	0.66	0.32	0.48	0.63	0.76
P4	3.68	0.55	0.28	0.50	0.64	0.78
P5	2.72	0.40	0.27	0.68	0.71	0.96

single crystals with different oxygen contents. The data related to the single crystal with optimum oxygen content indicate that the slope of the in-plane electrical resistivity, $\rho_{ab}(T)$, in the T-linear part, is $A_{sc} = 1.84\ \mu\Omega$ cm/K and that the electrical resistivity at 300 K is $\rho_{ab}(T) \approx 496\ \mu\Omega$ cm.[21]

Therefore, both α_n and ρ_{wl} can be obtained by using the appropriate expressions,[13]

$$\alpha_n = \frac{A_{sc}}{A}, \tag{4}$$

and

$$\rho_{wl} = \alpha_n \rho(0), \tag{5}$$

where A is the slope of the $\rho(T)$ curve in the T-linear region ($T \geq T_\rho^*$) and $\rho(0)$ the residual electrical resistivity at $T = 0$. Both parameters were obtained by fitting the electrical resistivity data to the typical linear dependence $\rho(T) = AT + \rho(0)$. The best fitting parameters by using the above linear dependence are displayed in Table II.

As inferred from the analysis of Eq. (5), the residual electrical resistivity $\rho(0)$ can not be considered as the actual intergranular electrical resistivity of the sample. Moreover, $\rho(0)$ quantifies the influence of both the texture and microstructural defects on the magnitude of the intergranular electrical resistivity of the polycrystalline sample.

The calculated values of α_n and ρ_{wl}, by using Eqs. (4) and (5), are given in Table II. As expected from the previous analysis, ρ_{wl} decreases appreciably (~ 30 %) with increasing compacting pressure, indicating an improvement of the intergranular component of ρ. Such a decrease in ρ_{wl} with increasing compacting pressure is mainly related to two mechanisms: an increase of the degree of texture and a decrease of microstructural defects.

In order to gain further information regarding the above mechanisms, we tentatively try to separate both contributions from the estimated values of α_n. Such a separation requires, according to Eq. 3, the determination of f or α_{str}. As far as this point is concerned, Díaz *et al.* [13] have proposed an experimental procedure based on measurements of the paracoherent electrical resistivity of polycrystalline samples, ρ_p, to

determine these parameters. In such a procedure, it has been assumed that the sample is in the so-called paracoherent state. This means that the grains are in the superconducting state but the intergranular junctions remain in the normal-state. Under these circumstances, the first term in Eq. (2) can be neglected and effects arising from the misalignment of grains become irrelevant, i. e., $f = 1$ and $\alpha_n = \alpha_{str}$. In this case Eq. (2) is altered and rewritten as

$$\rho_p = \frac{1}{\alpha_{str}}\rho_{wl}, \tag{6}$$

where ρ_p is the paracoherent electrical resistivity. By using Eq.(6) in combination with the values of both ρ_p and ρ_{wl}, an estimate of α_{str} is possible. We have performed these estimates and the obtained values are displayed in Table II. As can be inferred from Eq. (6), the observed decrease in ρ_p values with increasing compacting pressure (see Table I) is related to a similar behavior observed in ρ_{wl} and the progressive increase of α_{str} (~ 40 %), which in turn indicates the reduction of microstructural defects. In addition, one may to estimate the values of the grain misalignment factor f by using Eq. (3), knowing both α_n and α_{str}. As displayed in Table II, the grain misalignment factor f increases from $f \sim 0.58$ to $f \sim 0.71$ for samples **P1** and **P5**, respectively. These results indicate an appreciable increase in the degree of texture with increasing compacting pressure and are in excellent agreement with both XRD and SEM data.

On the other hand, by combining the observed T-linear behavior in the $\rho(T)$ dependence (see Fig. 4) with band-theory arguments, it is possible to obtain additional information regarding the effects of the compacting pressure on the normal-state transport properties.[7] Based on the behavior of A an important information regarding the strength of the electron-phonon interaction can be obtained. By considering that the T-linear behavior of $\rho(T)$ curve is mainly caused by the electron-phonon scattering, then the transport electron-phonon coupling constant λ_{tr} can be estimated from the expression[7]

$$\lambda_{tr} = \frac{\hbar\omega_p^2 A}{8\pi^2 k_B} = 0.246(\hbar\omega_p)^2 A, \tag{7}$$

where k_B is the Boltzmann constant, $\hbar\omega_p$ is the plasma energy expressed in eV, and A is expressed in $\mu\Omega$ cm/K (see Table II). Assuming that the London penetration depth λ_L for the BSCCO system is ~ 2100 Å,[22] then the plasma frequency can be estimated by using the relation $\omega_p = c/\lambda_L$, where c is the velocity of light, yielding $\hbar\omega_p = 0.893$ eV. Additionally, from the electrical resistivity measurements one can also estimate the mean free path of the carriers, l, following the equation:[7]

$$l(T) = \frac{4\pi v_F}{\omega_p^2 \rho(T)} = \frac{4.95 \times 10^{-4} v_F}{(\hbar\omega_p)^2 \rho(T)}, \tag{8}$$

where v_F is the Fermi velocity, which for BSCCO materials is $\sim 2.5 \times 10^7$ cm s^{-1},[22] and $\rho(T)$ is given in $\mu\Omega$ cm.

We mention that in Ref. 7, values of $\rho(T)$ data have been corrected by a factor $\beta = \rho/\rho_{ab}$ in order to separate the *ab*-plane electrical resistivity from the measured electrical resistivity of polycrystalline samples. A constant value of $\beta \sim 2$ was derived, by comparing the transport data with those from high-quality ceramic and epitaxial thin films. Here we assume that such a correction factor must take into account the granular features of ceramic samples and adopt the form $\beta = 1/\alpha_n$.
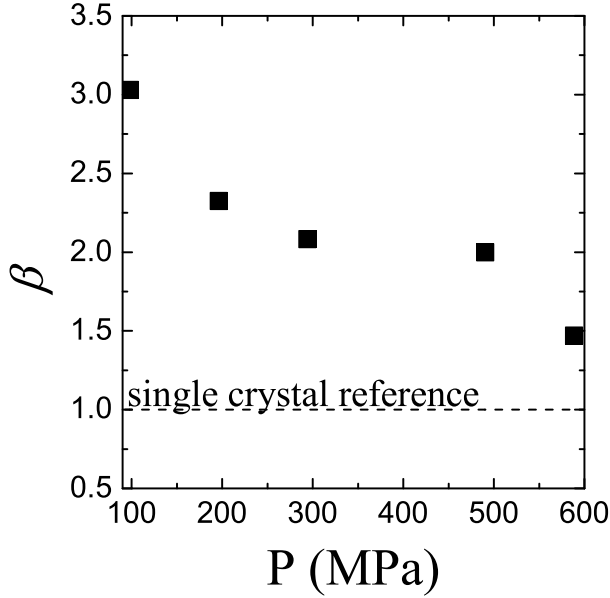

FIG. 8: Compacting pressure dependence of the correction factor β. The dashed line indicates $\beta = 1$, a value corresponding to a single crystal specimen.

Figure 8 displays the compacting pressure dependence of the correction factor β. It was found that the latter decreases from $\beta \sim 3$, for the sample **P1**, to $\beta \sim 1.5$ for the sample **P5**, exhibiting a clear tendency to $\beta = 1$, a value obtained from a single crystal specimen. This result strong suggests that samples subjected to an optimally textured process can be used to obtain appropriated values of the transport electron-phonon constant as well as single crystal materials. Then, by using Eq. (7) and (8) we obtained for the sample **P5** values of $\lambda_{tr} = 0.53$ and $l(300\ \mathrm{K}) = 12.7$ Å. Similarly, the results obtained from the data of Bi-2223 single crystals[21] were $\lambda_{tr} = 0.37$ and $l(300\ \mathrm{K}) = 31$ Å, respectively. Good agreement between estimates of the electron-phonon coupling constant are observed. Also, values comparable with the one obtained for the sample **P5** have been estimated in other High-T_c materials as $\lambda_{tr} = 0.1$ - 0.6 in Y-123, [7, 23, 24] $\lambda_{tr} \sim 0.3$ in LaSrCuO,[7] and $\lambda_{tr} \sim 0.17$ in Ru-1222.[25] Values of λ_{tr} in this range indicate a weak electron-phonon interaction in Bi-2223.

We have also found that $l(300\ \mathrm{K})$ for the sample **P5** is actually higher than the typical Cu-O bond-length of ~ 2 Å in these cuprates. This lends credence to our analysis since no evidence of saturation in $\rho(T)$ has been observed close to 300 K. However, the value of $l(300\ \mathrm{K})$ of ~ 12.7 Å for the sample **P5** is ~ 3 times lower than the one derived for single crystals (31 Å) by using the same procedure. It seems that such a dif-ference is certainly related to the influence of the intergranular electrical resistivity ρ_{wl}.

In order to evaluate the influence of the actual intergranular electrical resistivity, ρ_{wl}, on the mean free path, let us estimate l by neglecting the contribution arising from ρ_{wl} in Eq. (2). By taking the data belonging to the sample **P5** and assuming $\alpha_{str} \approx 1$ (see Table II), one obtains, by using Eq. (8), $l(300\ \mathrm{K}) \approx 21$ Å. This value of $l(300\ \mathrm{K})$ is closer to the one estimated for Bi-2223 single crystals of $l \approx 31$ Å, and over 1.5 times higher than the previous estimate of l in which the intergranular component of $\rho(T)$ has been considered.

V. CONCLUSIONS

In summary, we have carried out a systematic study on the influence of the uniaxial compacting pressure on the transport properties of $Bi_{1.65}Pb_{0.35}Sr_2Ca_2Cu_3O_{10+\delta}$ ceramic samples subjected to different compacting pressures before the last heat-treatment. Based on the linearity of the electrical resistivity curves and applying appropriate corrections, we have estimated both the transport electron-phonon coupling constant, λ_{tr}, and the mean free path, l. We have found that the extracted λ_{tr} values in well-compacted samples are in good agreement with similar estimates for single crystals. On the other hand, an appreciable difference was found in the case of the mean free path, l. Such a difference is certainly related to the intergranular electrical resistivity, which is an intrinsic feature of polycrystalline samples. In addition, contributions for the electrical resistivity arising from both the degree of texture and microstructural defects were extracted from a precise analysis of the $\rho(T)$ dependence by using current models. It was found that increasing compacting pressure results in an increase of both the degree of texture and the grain connectivity of the samples. We have also observed that the electrical resistivity curves in the normal-state region deviate from linearity at $T^* \sim 235$ K, a feature that points out changes in the density of states and is related to the opening of the pseudogap. Such an opening of the pseudogap was confirmed by powder magnetic susceptibility measurements performed in the same samples. The temperature of the pseudogap T^* resulted to be independent of the applied compacting pressure. This is an expected result considering that changes in the compacting pressure mainly affect the morphology of the grains, but the intragranular properties remain essentially the same.

---

[1] H. Hilgenkamp and J. Mannhart, Rev. Mod. Phys. **74**, 485 (2002).

[2] T. T. Tan, S. Li, H. Cooper, W. Gao, H. K. Liu and S. X. Dou, Supercond. Sci. Technol. **14** 471 (2001).

[3] H. K. Liu, Y. C. Guo, and S. X. Dou, Physica B **194**, 1931 (1994).

[4] H. K. Liu, W. M. Chen, A. Polyanskii, Y. C. Guo, G. Mac-Caughey, S. X. Dou, D. Larbalestier, and M. Apperley, Physica C **341**, 2547 (2000).

[5] W. M. Chen, Y. C. Guo, G. MacCaughey, M. Apperley, H. K. Liu, and S. X. Dou, Physica C **354**, 349 (2001).

[6] P. Muné, E. Govea-Alcaide, and R. F. Jardim, Physica C **384**, 491 (2003).

[7] M. Gurvitch and A. T. Fiory, Phys. Rev. Lett. **59**, 1337 (1987).

[8] J. L. Tallon and J. W. Loram, Physica C **349**, 53 (2001).

[9] V. J. Emery and S. A. Kivelson, Nature (London) **374**, 434 (1995).

[10] T. Fujii, T. Watanabe, and A. Matsuda, Physica C **357**, 173 (2001).

[11] D. C. Johnston, Phys. Rev. Lett. **62**, 957 (1989).

[12] C. Allgeier and J. S. Schilling, Phys. Rev. B **48**, 9747 (1993).

[13] A. Díaz, J. Maza, and F. Vidal, Phys. Rev. B, **55**, 1209 (1997).

[14] D. Goldschmidt, Phys. Rev. B **39**, 9139 (1989).

[15] D. Pandey, R. Mahesh, A. K. Singh, and V. S. Tiwari, Physica C **184**, 135 (1991).

[16] Y. Yamada, K. Anagawa, T. Shibauchi, T. Fujii, T. Watanabe, A. Matsuda, and M. Suzuki, Phys. Rev. B **68**, 54533 (2003).

[17] T. Ekino, S. Hashimoto, T. Takasaki, and H. Fujii, Phys. Rev. B **64**, 092510 (2001).

[18] A. A. Zhukov, D. A. Komarkov, and J. Mikovic, Cryogenics **32**, 1056 (1992).

[19] P. Muné, J. López, and E. Altshuler, Physica C **292**, 48 (1995).

[20] M. R. Cimberle, C. Ferdeghini, R. Flükiger, E. Giannini, G. Grasso, D. Marrè, M. Putti, and A. S. Siri, Physica C **251**, 61 (1995).

[21] T. Fujii, private communication.

[22] M. Chiao, R. W. Hill, C. Lupien, L. Taillefer, P. Lambert, R. Gagnon, and P. Fournier, Phys. Rev. B **62**, 3554 (2000).

[23] B. Friedl, C. Thomsen, and M. Cardona, Phys. Rev. Lett. **65**, 915 (1990).

[24] T. S. Nunner, J. Schmalian, and K. H. Bennemann, Phys. Rev. B **59**, 8859 (1999).

[25] M. T. Escote, V. A. Meza, R. F. Jardim, L. Ben-Dor, M. S. Torikachvili, and A. H. Lacerda, Phys. Rev. B **66**, 144503 (2002).